

# Thermomagnetic Convection of Magnetic Fluids in a Cylindrical Geometry

Adrian Lange

Institut für Theoretische Physik, Universität Magdeburg, Postfach 4120, D-39016 Magdeburg,  
Germany

## Abstract

The thermomagnetic convection of magnetic fluids in a cylindrical geometry subjected to a homogeneous magnetic field is studied. The study is motivated by a novel thermal instability [W. Luo et al., Phys. Rev. Lett. 82, 4134 (1999)]. A model system—a composite cylinder with inner heating—is considered which reflects the symmetry of the experimentally setup. The general condition for the existence of a potentially unstable stratification in the magnetic fluid is derived. Within a linear stability analysis the critical external induction for the onset of thermomagnetic convection is determined for dilute and nondilute magnetic fluids. The difference between both thresholds allows to test experimentally whether a test sample is a dilute fluid or not.

Contact author: Adrian Lange, Fax: +49-391-6711205

email: [adrian.lange@physik.uni-magdeburg.de](mailto:adrian.lange@physik.uni-magdeburg.de)

# 1 Introduction

Magnetic fluids (MFs) are superparamagnetic fluids formed by a stable colloidal suspension of ferromagnetic nanoparticles dispersed in a carrier liquid [1]. The behaviour of MFs is characterized by the complex interaction of their hydrodynamic and magnetic properties with external forces. For the phenomenon of thermomagnetic convection these forces are a temperature gradient and a magnetic field. Most studies consider the geometry of a horizontal layer which is simultaneously subjected to a vertical temperature gradient and either to a constant vertical magnetic field [2, 3, 4] or to a vertical magnetic field with a constant gradient [5]. Studies for a cylindrical geometry are few [6, 7] and focus on the thermomagnetic convection under microgravity [8].

The present analysis of thermomagnetic convection in a cylindrical geometry is motivated by a recently observed novel convective instability. In [9, 10] a horizontal layer of MF between two glass plates is locally heated by a focused laser beam. It passes perpendicularly through the layer in the presence of a homogeneous vertical magnetic field. The absorption of the light by the fluid generates a temperature gradient and subsequently a refractive index gradient. This gradient is optically equivalent to a diverging lens, leading to an enhancement of the beam divergence. As a result, a stationary diffraction pattern of concentric rings is observed for zero magnetic field. Above a certain threshold of the magnetic field, the circular rings are replaced by polygonally shaped patterns which switch among different shapes alternatively. Based on numerics it was stated that the characteristic time scales for mass and thermal diffusion are equal [9]. Thus thermal conduction and thermal diffusion contribute equally to the formation of the diverging lens. The polygonally shaped diffraction patterns were interpreted as 'fingerprints' of vertical convection columns [10].

Both claims are controversial due to the following reasons. An analysis of the physical quantities reveals that both characteristic time scales are several orders of magnitude apart (below and [11]). Direct spatial temperature measurements [12] and independent measurements of all relevant material parameters for organic dispersions [13] showed that the ring pattern is

essentially caused by the temperature contribution and not by the concentration contribution. The determination of the relevant time scales confirmed that the experiment is dominated by the characteristic time for convection. Presently there is no sound theoretical description for the dependence of the size of the outmost of the concentric rings on the laser power (see Fig. 2 in [13]).

A major hindrance of the studied system in [9, 10] is that it is almost impossible to gain information about the spatial distribution of temperature and concentration inside the MF layer. Due to the lack of sound internal information many hypotheses can be brought forward to explain the experimental results. Among them is the recent discussion whether the shape instability of a hot nonmagnetic bubble surrounded by MF can be accounted for the observed phenomena [14, 15].

This situation motivates the present work in which a model system is studied which reflects the essentials of the experimental setup. These are the axis-symmetry of the heating and the finite height and width of the layer. The aim is to determine the necessary conditions and the critical magnetic inductions for the appearance of axial convection columns. Thus the focus is on the general requirements for thermomagnetic convection in an axis-symmetric heated system.

This paper is organized as follows: The system and the relevant equations of the problem as well as the condition for a potentially unstable stratification in the fluid are displayed in the next section. Based on a linear stability analysis (Sec. III), the results are presented and discussed in Sec. IV. In the final section, the results are summarized.

## 2 Model and Equations

The model system is given by a composite, circular cylinder of height  $h$  which consists of three parts. The inner cylinder of radius  $R_1$ , constant temperature  $T_1$ , and constant susceptibility ( $T_1$ ) is surrounded by a middle cylinder of radius  $R_2$ . In the gap  $R_2 - R_1$  the temperature decreases to  $T_0 < T_1$  and consequently  $\chi$  is a spatially varying quantity,  $\chi = \chi(r)$ . The

outer cylinder has the radius  $R_{out}$ , where in the region  $R_{out} - R_2$  the constant temperature  $T_0$  and constant susceptibility  $\chi(T_0)$  is present. The whole system is subjected to a homogeneous vertical magnetic field and its effective susceptibility is given by

$$\chi_e = \frac{1}{R_{out}} \left[ R_1 \chi(T_1) + (R_2 - R_1) \int_{R_1}^{R_2} dr \chi(r) \right] + (R_{out} - R_2) \chi(T_0) : \quad (1)$$

In the presence of a uniform external magnetic induction  $B_{ext}$ , the internal field in the gap is given by  $H_{int} = B_{ext}/\mu_0(1 + N)$ . The susceptibility of the MF is  $\chi = \chi_L(1 + \chi_1\chi_L)$ , where  $\chi_L$  is the susceptibility according to Langevin's theory which assumes non-interacting particles. Higher order terms in  $\chi_L$  are included in order to determine the magnetic (or Kelvin) force density beyond the dilute limit  $\chi = \chi_L$ . The coefficient  $\chi_1$  was determined in different microscopic models [16, 17, 18] which all provide the same value  $\chi_1 = 1/3$ . The demagnetization factor  $N$  accounts for the finite size of the composite cylinder and is a function of the height-to-diameter ratio  $h = h/(2R_{out})$  and the effective susceptibility  $\chi_e$  [19]. The Kelvin force follows then as [20]

$$f_K = -\frac{B_{ext}^2}{2\mu_0} \chi_L \frac{d\chi_L}{dL} ; \quad (2)$$

where

$$\chi_L = \frac{\chi_L^2 fN + \chi_1 [3N - \chi_L(1 + \chi_1\chi_L) - 1]g}{(1 + N)^3} ; \quad (3)$$

Considering MFs as binary mixtures, it is necessary to evaluate the influence of temperature and concentration on pattern phenomena by analyzing the corresponding time scales. These are the characteristic time for convection  $t_c = L_c^2/\nu$  and for mass diffusion  $t_d = L_d^2/D$ , where  $L_c$  ( $L_d$ ) is the typical length for convection (diffusion),  $\nu$  the thermal diffusivity, and  $D$  the mass diffusion coefficient. Using the data given in [1, 9], one gets  $\nu \approx 4 \cdot 10^{-8} \text{ m}^2 \text{ s}^{-1}$  and  $D \approx 8 \cdot 10^{-12} \text{ m}^2 \text{ s}^{-1}$ . Except in specially designed geometries as in [21], where  $L_c \ll L_d$ , the characteristic time for diffusion is of three orders of magnitude larger than the characteristic time for convection. Since in our model both length scales are equal to the gap width  $R_2 - R_1$ , diffusion phenomena can be neglected.

The system is governed by the equation of continuity, the Navier-Stokes equations, and the equation of heat conduction for the MF which are in nondimensional form

$$\text{div } \mathbf{v} = 0; \quad (4)$$

$$\frac{\partial \mathbf{v}}{\partial t} + (\mathbf{v} \cdot \text{grad}) \mathbf{v} = -P (-\text{grad } p + \mathbf{v}) + M F_L \frac{\text{grad } T}{T}; \quad (5)$$

$$\frac{\partial T}{\partial t} + (\mathbf{v} \cdot \text{grad}) T = T; \quad (6)$$

where the Prandtl number  $P = \frac{\eta}{\kappa}$  characterizes the fluid and the magnetization number  $M = B_{\text{ext}}^2 (R_2 - R_1)^2 / (\mu_0 \eta^2)$  tunes the external excitation. Denoting  $\eta$  as kinematic viscosity, the velocity  $\mathbf{v} = (u; v)$  is scaled with  $\eta (R_2 - R_1)$ , time with  $(R_2 - R_1)^2 / \eta$ , temperature with  $(T_1 - T_0)$ , and pressure  $p$  with  $\eta (R_2 - R_1)^2$ .  $\nabla$  and  $\text{grad}$  are the corresponding differential operators in the plane cylindrical coordinates  $r$  and  $\theta$ . Rigid boundary conditions are assumed for the velocity at the inner and outer radius of the gap,  $u = \partial_r u = 0$  at  $r = 1$  and  $r = 1/(1 - \epsilon)$ , where the radii ratio is given by  $\epsilon = R_1/R_2$ . The temperature is assumed to be constant at each boundary,  $T(r=1) = T_1$  and  $T(r=1/(1 - \epsilon)) = T_0$ .

Since the Kelvin force is the only destabilizing force present in the system, one has to determine which profile leads to a potentially unstable stratification in the fluid. For heating at the inner radius, the required profile is given in Fig. 1 (a): the  $r$ -component of the Kelvin force density has to act inwards and its absolute value increases monotonically outward. With such a profile a fluid volume at the distance  $r + \Delta r$  (solid rectangle in Fig. 1 (b)) experiences a larger force towards the center compared to a fluid volume at the distance  $r$  (dashed rectangle). Moving the latter fluid volume from  $r$  to  $r + \Delta r$  (dot-dashed rectangle) results in an effective force which points in the direction of the displacement (indicated symbolically by the subtraction of the arrows in Fig. 1 (b) bottom). This force may enhance small displacements of warmer fluid volumes towards cooler regions and thus making the stratification potentially unstable.

The above argument has to be tested for the quiescent conductive state which is given by  $\mathbf{v}_G = 0$  and  $T_G = T_0 + (T_1 - T_0) \ln[r(1 - \epsilon)] / \ln 1/(1 - \epsilon)$ . Applying the condition for a destabilizing

force profile to the r-component of the Kelvin force density in Eq. (2) leads to the condition

$$\frac{\partial}{\partial r} f_{K,r} = -M \frac{\partial_r T}{T} \frac{\partial (f_L F_L)}{\partial L} + M F_L \frac{\partial_r^2 T}{T} < 0$$

for all  $r \in [r_1, r_2]$  : (7)

Since  $\partial_r f_{K,r}$  is a monotonously decreasing function of  $r$ , it is sufficient if  $\partial_r f_{K,r} < 0$  at  $r = r_1$  in order to fulfill the condition (7). Depending on the temperatures  $T_1$  and  $T_0$ , the Langevin susceptibility  $f_L$ , the demagnetization factor  $N$ , and  $\beta_1$  the condition (7) entails that the radii ratio has to be larger than a critical value. For realistic temperatures  $T_1$  above a room temperature of  $T_0 = 300$  K, it becomes clear that this condition is met only in a narrow gap (see Fig. 2). This is plausible because the nonlinear temperature profile  $T_G = \ln[r(1 - \beta_1)]$  can be well approximated in a small gap by a linear profile which always satisfies the requirement (7) if  $\beta_1 = 0$ .

### 3 Linear Stability Analysis

Exploiting the smallness of the gap, in the linear stability analysis terms as  $\partial_r (\partial_r + 1/r)$  are approximated by  $\partial_r^2$  and the new variable  $u = r - r_1 = (1 - \beta_1)$  is introduced. All small disturbances from the ground state are decomposed into normal modes, i.e. into components of the form  $[u; p; T] = e^{nt} \cos(l\varphi) [u(\varphi); p(\varphi); T(\varphi)]$  and  $v = e^{nt} \sin(l\varphi) v(\varphi)$ , respectively. The nondimensional growth rate is denoted by  $n$  and  $l$  is the azimuthal wave number. For marginal stability,  $n = 0$ , the differential equations to solve are

$$\frac{\partial^2}{\partial u^2} u - \frac{2}{l^2} \frac{\partial^2}{\partial u^2} u = -\frac{2M}{P} f_L \frac{T}{T_G^2} \frac{\partial T_G}{\partial u}; \quad (8)$$

$$\frac{\partial^2}{\partial u^2} T = u (T_0 - T_1); \quad (9)$$

where  $\beta_1 = (1 - \beta_1)l^2$  and

$$f_L = \frac{\partial F_L}{\partial L} = \frac{\frac{2}{L}}{(1 + N)^4} [6N^2 \frac{2}{L} \frac{3}{L} (1 + \beta_1 L) + 4N \frac{2}{L} \frac{1}{L} (N - 4\beta_1) + \frac{2}{L} (N - 10\beta_1) + 2\beta_1 - 2N]; \quad (10)$$

In order to satisfy the four boundary conditions  $u = 0$  at  $x = 0; 1$ , the ansatz

$$u(x) = \sum_{m=1}^K P_m \sinh(a_m x) + B_m \cosh(a_m x) + C_m \sin(b_m x) + D_m \cos(b_m x) \quad (11)$$

with  $a_m = \sqrt{q_m^2 + \frac{1}{2}}$  and  $b_m = \sqrt{q_m^2 - \frac{1}{2}}$  is chosen.  $q_m$  is a root of a transcendental equation and the constants  $B_m$ ,  $C_m$ , and  $D_m$  are determined by the boundary conditions (for details see [22]). With Eq. (11) the solution of Eq. (9) reads  $T(x) = \sum_{m=1}^K P_m T_m(x) + C_1 e^{x/2} + C_2 e^{-x/2}$ .  $T_m(x)$  is the solution of the inhomogeneous equation (due to its lengths not given here) and the constants  $C_1$  and  $C_2$  are determined by the boundary conditions  $T = 0$  at  $x = 0; 1$ . Using Eq. (11) and the solution for  $T(x)$ , Eq. (8) can be approximately solved by the Galerkin method. Due to the good convergence, all presented results are based on the third approximation (see Table 1). For the calculations fluid parameters of EM G 901 are used:  $\rho = 1.53 \cdot 10^3 \text{ kg m}^{-3}$ ,  $\eta = 6.54 \cdot 10^{-6} \text{ m}^2 \text{ s}^{-1}$ ,  $\mu_L = 3$ , and  $\kappa = 4.2 \cdot 10^{-8} \text{ m}^2 \text{ s}^{-1}$  [23]. The temperature at the outer radius of the gap  $R_2 = 1 \text{ cm}$  is fixed at  $T_0 = 300 \text{ K}$ . The height of the composite cylinder is given by  $h = 1 \text{ cm}$  and the inner radius by  $r_1 = 1.01 \text{ cm}$  ( $\gamma_1 = 1.3; N = 1$ ). The choice of  $\gamma_1 = 1.3; N = 1$  (solid line in Fig. 2) ensures that for all following parameter sets the condition (7) is fulfilled.

## 4 Results and Discussion

Solving Eq. (8) with the Galerkin method and subsequently minimization with respect to the azimuthal wave number determines the critical external induction  $B_c$  and the corresponding wave number  $l_c$  (Figs. 3 and 4). Four different parameter sets were chosen: a dilute ( $\gamma_1 = 0$ ) and a nondilute ( $\gamma_1 = 1.3$ ) MF with  $R_{\text{out}} = 1 \text{ cm}$  ( $N = 1$ ) and  $R_{\text{out}}' = 3.33 \text{ cm}$ , respectively. The demagnetization factor  $N$  for the resulting height-to-diameter ratio  $h/d = 0.15$  and the effective susceptibility  $\chi_e$  of the composite cylinder accordingly to Eq. (1) is taken from the data given in [19].

Decreasing the temperature difference from  $T = 70 \text{ K}$  to  $T = 4 \text{ K}$  causes a dramatic increase in the critical induction of nearly three orders of magnitude (Fig. 3). With decreasing

temperature difference the critical radii ratio grows, i.e. the allowed gap becomes more narrow. Since the convection rolls prefer the same length scale in  $r$  and  $\theta$ -direction, much more rolls have to be driven in a very small gap. The energy for this effort comes from the external induction which is why it amplifies drastically for small  $T$  (Fig. 3).

Whereas the critical azimuthal wave number  $l_c$  is independent of  $(L)$  and  $N$  (Fig. 4), the critical induction varies. First the two thresholds for the case of an infinitely extended layer,  $R_{out} = 1$ , are compared. The inclusion of a quadratic term in the susceptibility with  $\chi_1 = 1/3$  results in a lower threshold for the onset of convection than in the dilute case  $\chi_1 = 0$  (solid and long-dashed line in Fig. 3). The difference between the thresholds is nearly the same value,  $B_c(\chi_1 = 1/3; N = 1) \approx 0.63 B_c(\chi_1 = 0; N = 1)$ , for all tested temperatures  $304 \text{ K} \leq T_1 \leq 370 \text{ K}$ .

Now the thresholds for the case of a finite layer with  $R_{out} \approx 3.33 \text{ cm}$  are compared. Contrary to the previous case, the threshold for a dilute uid (dot-dashed line in Fig. 3) is lower than for a nondilute uid (dotted line). Again the difference is almost constant over the entire temperature range,  $B_c[\chi_1 = 1/3; N(\epsilon = 0.15; \epsilon_e)] \approx 1.18 B_c[\chi_1 = 0; N(\epsilon = 0.15; \epsilon_e)]$ .

The relation of the different thresholds is caused by the value of  $f_L$  for the given combinations of  $N$ ,  $\chi_1$ , and  $L$ .  $f_L$  can be considered as a measure for the strength of the magnetic force in the gap: as higher the value of  $f_L$  as lower the critical external induction necessary to trigger the convection. Figure 5 shows the value of  $f_L$  for the four considered parameter sets. At  $L = 3$  the relation  $f_L(\chi_1 = 0; N = 1) < f_L(\chi_1 = 1/3; N = 1)$  (see cross-sections of the long-dashed and the solid line with the vertical solid line) is the reason that the threshold for the dilute uid is higher than for the nondilute uid. The opposite relation  $f_L[\chi_1 = 0; N(\epsilon = 0.15; \epsilon_e)] > f_L[\chi_1 = 1/3; N(\epsilon = 0.15; \epsilon_e)]$  (see cross-sections of the dot-dashed and the dotted line with the vertical solid line) causes the opposite relation for the thresholds in the case of a finite layer.

The physical reasons which cause these differences are the following. The Kelvin force is proportional to the magnetization in the magnetic uid. Thus as higher the magnetization is, as lower the external induction can be in order to generate the same strength of the mag-



netic force. In the infinite case, where  $N = 1$  is independent of  $\phi$ , a higher concentration of magnetic particles in the fluid leads to a higher magnetization and therefore to a lower threshold. In the finite case, the demagnetization factor depends on  $\phi$  [19] and is smaller for higher concentrations of magnetic particles than for lower concentrations. A higher demagnetization factor means a lower inner field and a higher magnetization, respectively. Therefore in the finite case an increase in the concentration results in two counteracting effects with respect to the magnetization. In the studied example of  $L = 3$  the influence of the demagnetization effect wins: the dilute fluid has the lower threshold. But for  $L > 3.2$  the direct influence of the concentration succeeds over the demagnetization effect. The nondilute fluid has the lower threshold (the dotted line is then above the dot-dashed line, see Fig. 5).

In the infinite and finite case the clear and measurable difference between the thresholds opens a very good opportunity to decide whether a test sample is a dilute fluid or not. Just by measuring the threshold for the onset of convection in the proposed model system the answer can be given. The critical induction depends on the fluid and system parameters as  $B_c = \frac{P}{R_2 - R_1}$ . By choosing fluids with low (high) density and thermal conductivity and a large (small) radius  $R_2$ , the threshold can be lowered (raised) corresponding to the experimentally available magnetic fields.

The major obstacle in order to compare the results with the experimental data in [10] is the lack of an experimentally determined spatial profile of the temperature inside the sample. Therefore it is not possible to extract an estimation what might be the values of  $R_1$  and  $R_2$  in the experiment. Nevertheless the calculated values indicate that really high critical external inductions are necessary to trigger vertical convection rolls by a pure radial temperature gradient. The threshold for the induction reaches extremely high values if one extrapolates towards radii in the range of hundreds of micrometers, not unlikely due to the focused laser beam used in the experiment [9, 10]. This leads to the conclusion that vertical convection rolls due to a pure radial temperature gradient are unlikely to account for the observed phenomena of polygonally shaped diffusion patterns.

Due to the lack of information from inside the sample, it is not clear whether the temperature profile in the experimental sample is purely radial. There are hints in [24] that due to the absorption along the way of the laser beam a vertical temperature distribution exists as well. A further cause for an axial temperature gradient is the heat loss through the glass plates by which the MF layer is sandwiched. If such a vertical temperature gradient comes into play, concentration gradients due to the Soret effect may become important. The relative influence of temperature and concentration gradients is strongly affected by the relation of the characteristic times  $t_c$  and  $t_d$  which depend quadratically on the lengths  $L_c$  and  $L_d$ , respectively. With a radial and a vertical temperature gradient present, it becomes even more important to have reliable data of the internal profiles to estimate these lengths.

Two differences between the model and the motivating experiment should be noted. The constant temperature  $T_1$  for the inner cylinder is not given in the experiment. How much the temperature varies in this inner area is not known. The numerical calculations in [9] suggest a difference of about 15 K. The thresholds were calculated for rigid boundaries whereas in the experiment the fluid layer boundary is free. For thermal convection in a rotating layer of magnetic fluid the influence of rigid and free boundaries on the threshold was studied in [4]. Considering the case of zero rotation, the thresholds differ by not more than 20% (see Figs. 3 and 4 in [4] for rotation number  $T \neq 0$ ). With respect to the above mentioned major obstacle, these differences may alter the results only marginally.

## 5 Summary

A model system of a composite cylinder of finite size with axis-symmetrical temperature distribution is presented. Using the Kelvin force density (2,3) a general condition (7) is derived for which a potentially unstable stratification exists if the inner cylinder is heated. Depending on the temperature difference, the size of the composite cylinder and the dilute or nondilute character of the magnetic fluid, the critical gap sizes are calculated. The general result is that only in a narrow gap the requirement for a potentially unstable stratification is met. Exploiting

this property, a linear stability analysis is performed in order to determine the critical external induction for the onset of thermomagnetic convection. With decreasing temperature difference, the critical induction increases dramatically. The reason is that for smaller temperature differences which demand smaller gaps in order to fulfill condition (7), much more convection rolls have to be driven. The driving of these many rolls causes the drastic increasing of the critical induction. The distinct difference between the threshold for dilute and nondilute magnetic fluids allows to use the considered system for an experimental determination whether a test fluid is a dilute or nondilute one.

The rather high external induction, needed to stimulate the convection flow, leads to the conclusion that vertical convection rolls due to a pure radial temperature gradient are unlikely to account for the observed deflection patterns. The consideration of a vertical temperature gradient entails that concentration gradients may become relevant. To answer this question the characteristic time for the diffusion with respect to whose for convection has to be re-estimated. Because they will not be necessarily apart by orders of magnitude as in the case of a pure radial temperature gradient. Also different convection patterns can be expected with the presence of a vertical temperature gradient. In order to come to a correct statement about the contribution of mass and thermal diffusion to the deflection patterns in magnetic fluids, spatial temperature measurements and independent measurements of all relevant material parameters as in [12, 13] for an organic dispersion are highly desirable.

## References

- [1] R. E. Rosensweig, *Ferrohydrodynamics* (Cambridge University Press, Cambridge, 1985).
- [2] B. A. Finlayson, "Convective instability of ferromagnetic fluids", *J. Fluid Mech.* 40, 753 (1970).
- [3] L. Schwab, U. Hildebrandt, and K. Stierstadt, "Magnetic Benard convection", *J. Magn. Magn. Mat.* 39, 113 (1983); L. Schwab and K. Stierstadt, "Field-induced wavevector-

- selection by magnetic Benard-convection", *ibid.* 65, 315 (1987); L. Schwab, "Thermal convection in ferro fluids under a free surface", *ibid.* 85, 199 (1990).
- [4] G. K. Auerhammer and H. R. Brand, "Thermal convection in a rotating layer of magnetic fluid", *Eur. Phys. J. B* 16, 157 (2000).
- [5] J. Huang, B. F. Edwards, and D. D. Gray, "Magnetic control of convection in nonconducting paramagnetic fluids", *Phys. Rev. E* 57, R29 (1998); "Thermally convective instability of paramagnetic fluids in a nonuniform magnetic field", *ibid.* 5564.
- [6] H. Morimoto, T. Maekawa, and M. Ishikawa, "Linear stability analysis of magnetic Rayleigh-Benard convection", *Adv. Space Res.* 22, 1271 (1998).
- [7] A. Zebib, "Thermal convection in a magnetic fluid", *J. Fluid Mech.* 321, 121 (1996).
- [8] S. Odobach, "Drop tower experiments on thermomagnetic convection", *Microgravity sci. technol. V I*, 161 (1993).
- [9] T. Du and W. Luo, "Nonlinear optical effects in ferro fluids induced by temperature and concentration cross coupling", *Appl. Phys. Lett.* 72, 272 (1998).
- [10] W. Luo, T. Du, and J. Huang, "Field-induced instabilities in a magnetic fluid", *Phys. Rev. Lett.* 82, 4134 (1999).
- [11] M. I. Shliomis and M. Souhar, "Self-oscillatory convection caused by the Soret effect", *Europhys. Lett.* 49, 55 (2000).
- [12] W. Schaertl and C. Roos, "Convection and thermophoresis of colloidal gold tracers by light scattering", *Phys. Rev. E* 60, 2020 (1999).
- [13] R. Spill, W. Kohler, G. Lindenblatt, and W. Schaertl, "Thermal diffusion and Soret feedback of gold-doped polyorganosiloxane nanospheres in toluene", *Phys. Rev. E* 62, 8361 (2000).

- [14] M . I. Shliomis, \Comment on Novel convective instabilities in a magnetic fluid", Phys. Rev. Lett. 87, 059801 (2001).
- [15] W . Luo, T . Du, and J. Huang, \Luo, Du, and Huang reply", Phys. Rev. Lett. 87, 059802 (2001).
- [16] L. Onsager, \Electric moments of molecules in liquids", J. Am . Chem . Soc. 58, 1486 (1936).
- [17] M . S. Wertheim , \Exact solution of the mean spherical model for fluids of hard spheres with permanent electric dipole moments", J. Chem . Phys. 55, 4291 (1971); K . I. Morozov and A . V . Lebedev, \The effect of magneto-dipole interactions on the magnetization curves of ferrocolloids", J. Magn. Magn. Mat. 85, 51 (1990).
- [18] Y . A . Buyevich and A . O . Ivanov, \Equilibrium properties of ferrocolloids", Physica A 190, 276 (1992).
- [19] D . Chen, J . A . Brug, and R . B . Goldfarb, \Demagnetizing factors for cylinders", IEEE Trans. Magnetics 27, 3601 (1991).
- [20] A . Lange, \Kelvin force in a Layer of Magnetic Fluid", to appear in J. Magn. Magn. Mat., (2002).
- [21] T . Volker, E . Blums, and S . Odenbach, \Thermodynamic processes in ferro fluids", Magnetohydrodynamics 37, 274 (2001).
- [22] S . Chandrasekhar, Hydrodynamic and hydromagnetic stability, (Oxford Publications, New York, 1981), App. V .
- [23] The thermal diffusivity  $\kappa = (\kappa_p)$  can only be estimated since the producer does not report the heat capacity  $c_p$  and the thermal conductivity of the fluid EM G 901.
- [24] W . Luo, T . Du, and J. Huang, \Field-induced instabilities in a magnetic fluid", J. Magn. Magn. Mat. 201, 88 (1999).

Table 1: Critical external induction  $B_c$  in dependence of the order of approximation for  $N = 1$ .

$T_1$ [K]	$\alpha$	$B_c$ [T]			
		K = 1	K = 2	K = 3	K = 4
306	0	8.2527	8.2527	8.2502	8.2502
	1/3	5.1952	5.1952	5.1937	5.1937
320	0	0.4674	0.4674	0.4673	0.4673
	1/3	0.2942	0.2942	0.2942	0.2942
340	0	0.1178	0.1178	0.1177	0.1177
	1/3	0.07413	0.07413	0.07411	0.07411
370	0	0.04230	0.04229	0.04228	0.04228
	1/3	0.02663	0.02662	0.02662	0.02662

## Figure Captions

Figure 1: Required destabilizing force profile of the radial component of the magnetic force density  $f_{k,r}$  for inner heating (a). A fluid volume at the distance  $r + \Delta r$  (solid rectangle, (b)) experiences a larger force than a fluid volume at the distance  $r$  (dashed rectangle, (b)). Moving the latter volume from  $r$  to  $r + \Delta r$  (dot-dashed rectangle, (b)) results in an effective force which points in the direction of the displacement (dot-dashed arrow, (b)).

Figure 2: Region of potentially unstable and stable force profiles for a fixed outer temperature of  $T_0 = 300$  K and  $\chi_L = 3$ . The four different sets are  $\chi_1 = 0, N = 1$  (long-dashed line),  $\chi_1 = 0, N = 0.7$  (dot-dashed line),  $\chi_1 = 1=3, N = 1$  (solid line), and  $\chi_1 = 1=3, N = 0.7$  (dotted line), where the first and last one practically coincide.

Figure 3: Critical external induction  $B_c$  versus inner temperature  $T_1$  for a room temperature of  $T_0 = 300$  K. For a horizontally infinitely extended layer, i.e.  $R_{out} = 1$ , the inclusion of a quadratic term in the susceptibility with  $\chi_1 = 1=3$  (solid line) results in a lower threshold for the onset of convection than in the dilute case,  $\chi_1 = 0$  (long-dashed line). Contrary for  $R_{out} = 3.33$  cm, the critical induction for the dilute fluid (dot-dashed line) is lower than for the nondilute fluid (dotted line). The fluid parameters of the magnetic fluid EM G 901 and the size of the cylinder are given in the text.

Figure 4: Critical azimuthal wave number  $l_c$  versus inner temperature  $T_1$  for  $T_0 = 300$  K. With decreasing temperature difference the wave number, i.e. the number of convection rolls, increases dramatically from  $l_c = 14$  for  $T = 70$  K to  $l_c = 315$  for  $T = 6$  (K).

Figure 5:  $f_L$ , a measure for the strength of the magnetic force, versus the Langevin susceptibility  $\chi_L$ . The four different sets are  $\chi_1 = 0, N = 1$  (long-dashed line),  $\chi_1 = 1=3, N = 1$  (solid line),  $\chi_1 = 0, N = 0.15; \chi_e$  (dot-dashed line), and  $\chi_1 = 1=3, N = 0.15; \chi_e$  (dotted line). The vertical solid line at  $\chi_L = 3$  is a guide for the eye.

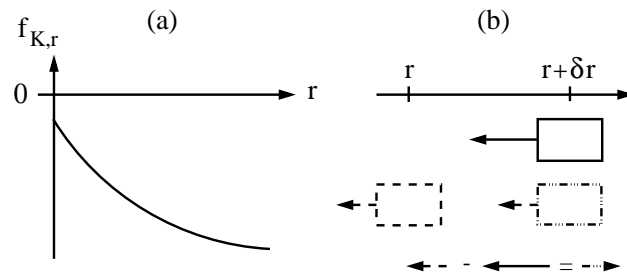


Figure 1: Lange, Physics of Fluids

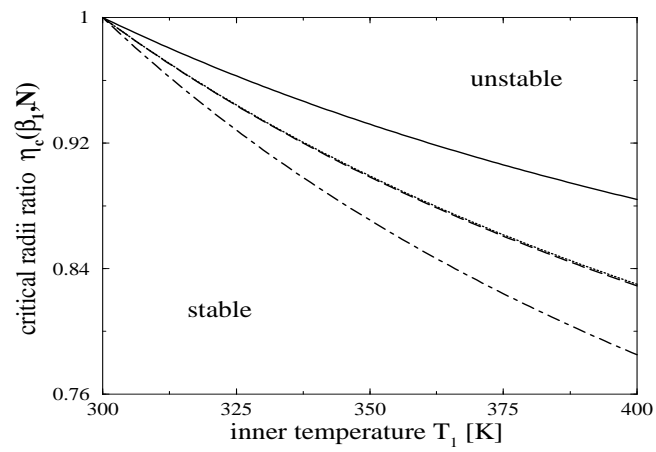


Figure 2: Lange, Physics of Fluids



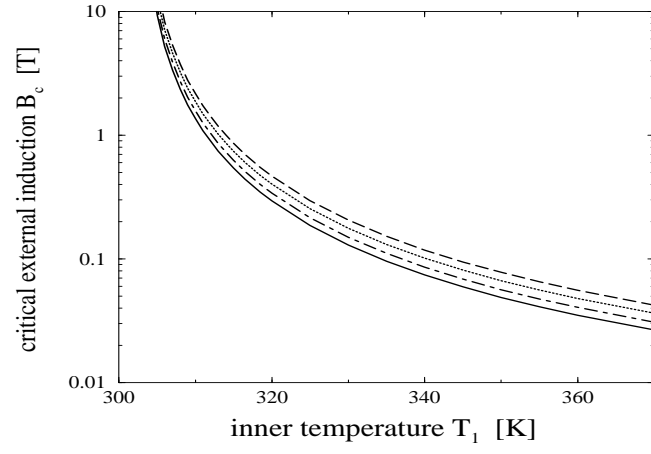


Figure 3: Lange, Physics of Fluids

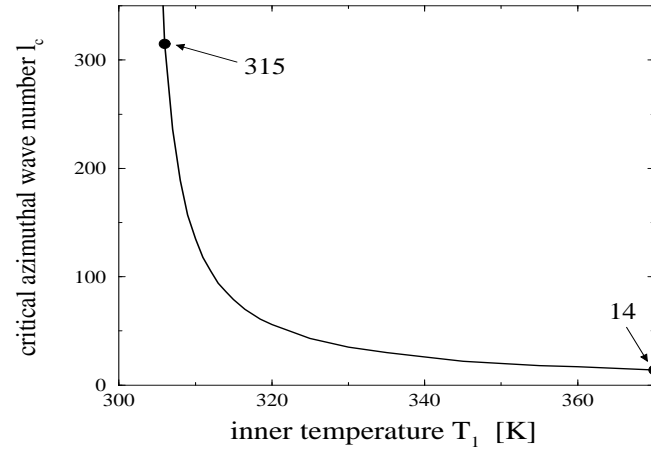


Figure 4: Lange, Physics of Fluids

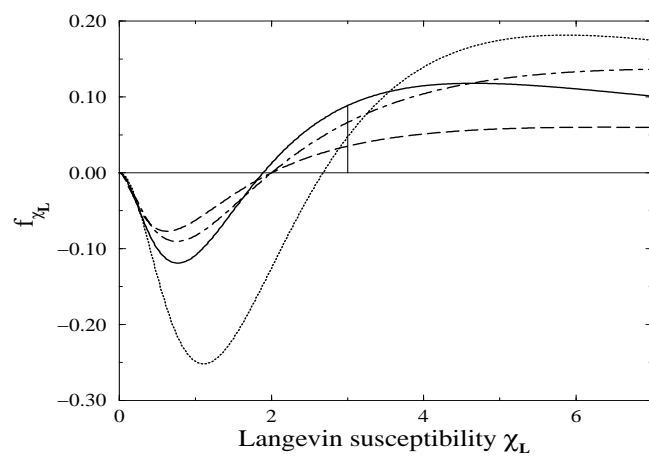


Figure 5: Lange, Physics of Fluids